Dalton Transactions

RSC Publishing

PAPER

View Article Online
View Journal | View Issue

Cite this: *Dalton Trans.*, 2013, **42**, 1406

Structural, magnetic and optical properties of an Fe^{III} dimer bridged by the meridional planar divergent *N,N'*-bis(salicyl)hydrazide and its photo- and electro-chemistry in solution†

Khaled Cheaib,[a] David Martel,[b] Nicolas Clément,[a] Fabrice Eckes,[a] Stéphanie Kouaho,[a] Guillaume Rogez,[c] Samuel Dagorne,[a] Mohamedally Kurmoo,[a] Sylvie Choua[d] and Richard Welter*[a]

Received 1st October 2012,
Accepted 29th October 2012

DOI: 10.1039/c2dt32310a

www.rsc.org/dalton

{$Fe^{III}Cl(DMF)_2$}$_2$(L) where L is *N,N'*-bis(salicyl)hydrazide has been synthesized as red crystals and characterized using single-crystal diffraction, infrared and UV-vis spectroscopies, and its magnetic properties studied. The dimeric unit in the structure is formed through the two meridional sets of divergent O, N, O coordinating atoms of the hexacoordinated and quadruply charged ligand. With the presence of the inversion symmetry the Fe atoms are strictly planar with the ligand. The magnetic exchange interaction is found to be antiferromagnetic with a $J = -5.98(3)$ cm^{-1} through the rare Fe–N–N–Fe pathway. Irradiation of the $FeCl_3$/H_4**L** red DMF solution in the visible region of the spectrum resulted in its complete discoloration and from which the unknown colorless salt [$Fe^{II}(DMF)_6$][$Fe^{II}Cl_4$] and the neutral ligand have been identified by single crystal diffraction. The UV-visible spectra of $FeCl_3$, H_4**L** and their mixture in DMF solution indicate that the iron complex is the absorbing species and the presence of the free ligand in the irradiated solution suggests that the ligand is potentially acting as a catalyst to the photoreduction of Fe^{III} to Fe^{II}, while electrochemistry points to a mixed-valent (Fe^{II}–Fe^{III}) intermediate in the process.

Introduction

Considerable efforts have been made over the past thirty years in understanding the magnetic exchange interaction between moment carriers in the solid-state.[1] In doing so a whole gamut of ligands has been employed to generate the chemical connection between near neighbours. A simple way of classification has been the number of non-magnetic atoms between neighbouring moment carriers.[2] From natural sources the ligand is usually oxide, which is a one-atom bridge, and the long-range magnetic ordering temperature is rather high (up to 800 K),[3] thus indicating strong exchange interaction. However, a similar connection using hydroxide reduces the dimensionality to two and the highest transition temperature is 60 K.[4] Azide and sometimes carboxylate can provide one-atom bridges but transition temperatures are still low (<100 K). However, a two-atom bridge such as cyanide favours linear connectivity and has produced several homo- and hetero-metallic Prussian-blue analogues where the transition temperature can exceed 300 K.[5] Other two-atom bridges that have been considered are pyrazole, triazole, and tetrazole for providing N–N connectivity between carriers and to a lesser extent dithione (S–S).[6] Extending to three-atom bridges there are dicyanamide,[7] azide,[8] carbonate,[9] oxalate,[10] carboxylate,[11] amongst others. These simple commercially available ligands have been very popular for they have provided many solids displaying long-range magnetic ordering at measurable temperatures.

In the last twenty years, there have been major interests in the development of organic ligands for accommodating high paramagnetic metal density and favourable and desired magnetic exchange pathways. For example Kahn *et al.* have developed the chemistry of oxamato derivatives,[12] which importantly provided divergent coordinating sites to generate

[a]*Laboratoire DECOMET, Institut de Chimie de Strasbourg, CNRS-UMR 7177, Université de Strasbourg, 4, rue Blaise Pascal, 67070 Strasbourg Cedex 1, France. E-mail: welter@unistra.fr; Fax: +33 68 85 12 29; Tel: +33 68 85 15 93*
[b]*Laboratoire d'Electrochimie et de Chimie Physique du Corps Solide, Institut de Chimie de Strasbourg, CNRS-UMR 7177, 4, rue Blaise Pascal, F-67070 Strasbourg Cedex 1, France*
[c]*I.P.C.M.S., CNRS-UMR 7504, Groupe des Materiaux Inorganiques, 23 Rue du Loess, BP 43, F-67034 Strasbourg Cedex 2, France*
[d]*Laboratoire POMAM, Institut de Chimie de Strasbourg, CNRS-UMR 7177, Université de Strasbourg, 4, rue Blaise Pascal, 67070 Strasbourg Cedex 1, France*
†Electronic supplementary information (ESI) available. CCDC 855119 (H_4**L**), 893268 & 893269 (iron complexes). For ESI and crystallographic data in CIF or other electronic format see DOI: 10.1039/c2dt32310a

infinite networks. This divergent nature of connecting ligands in molecular magnetism has since exploded to what we are now seeing in the metal–organic-framework field. The organic ligands with divergent coordinating sites have been useful to program the organization of paramagnetic centres within molecules; for example, Ruben *et al.*[13] have produced square grids while Peng *et al.*[14] made linear chains of up to nine metal centres. However, to date the simplest divergent ligand remains the oxalate anion and a whole family of magnetic networks made use of it. It is also interesting to note that nature has provided oxalate as well as inorganic non-magnetic ligands, such as sulfate, phosphate, molybdate, which are known to generate magnetic networks.[15]

One of the present waves of development of organic ligands is to use 2-salicyl-hydrazine moieties, where the O, N, O atoms can provide chelating sites.[16–20] This has been our motive for the last few years and it followed the observation of the strongest ferromagnetic exchange between two Mn^{III}.[21] The following works on Fe^{III} have found antiferromagnetic exchange but the compounds proved to be more interesting in solar energy conversion.[22,23] However, the ligands used in these studies were asymmetric and not with divergent coordination sites, which consequently ended as peripheral chelates. Others have shown that related ligands can produce ring clusters of up to six metal centres.[24] To extend this work, we have made use of the existing symmetric and potentially bis-meridional chelate ligand, *N*,*N*′-bis(salicyl)hydrazine (H_4**L**), that has been shown to form dimers with transition metals such as cobalt, nickel and zinc.[25–28] However, the magnetic properties have not been explored. Here, we present its coordination with Fe^{III} and the structural, optical and magnetic characterizations of a dimer, $(Fe^{III}Cl(DMF)_2)_2$L. Furthermore, we explore the photochemistry and the electrochemistry of the $Fe^{III}Cl_3$–H_4**L** couple in DMF solution in view of understanding the accompanied discoloration upon exposure to natural sunlight. The unknown $[Fe^{II}(DMF)_6][Fe^{II}Cl_4]$ and the free ligand, H_4**L**, resulted as colourless crystals from the decolorized solution have consequently been structurally characterized by diffraction. Electrochemistry and optical spectroscopy of H_4**L** and in the presence of Fe^{III} in DMF provide additional arguments for a proposed mechanism of the photo-reduction process.[29,30]

Experimental

General procedures

All manipulations were performed under aerobic conditions, using reagents and solvents as received. The NMR spectra were recorded using a Bruker AC 400 MHz NMR spectrometer at ambient temperature. $^{13}C\{^1H\}$ NMR spectra were recorded on a Bruker AVANCE 300 instrument at ambient temperature. ^{1}H-NMR chemical shifts are referenced to $SiMe_4$ and were determined by reference to the residual ^{1}H solvent peaks. IR spectra were recorded using a Nicolet 6700 FT-IR spectrometer in the region 4000–400 cm^{-1} and employing an ATR mode through a ZnSe crystal. Elemental analyses were performed by the "Service de microanalyses", Université de Strasbourg.

Synthesis of H_4L

The ligand was prepared using a modified procedure to those in the literature.[31] To a clear well-stirred solution of salicylic acid (2.72 g, 19.7 mmol) and salicylhydrazide (3 g, 19.7 mmol) in DMF (25 ml) was added drop-wise a solution of dicyclohexylcarbodiimide (4.7 g, 19.7 mmol) in DMF (15 ml). Butyl alcohol was added to catalyse the reaction. The resulting exothermic reaction caused the solution to become yellow and a white precipitate was formed. After four hours, the stirring was stopped and the white precipitate of dicyclohexylurea was removed by filtration. The filtrate was concentrated and then briefly heated under reflux to dissolve the precipitated material. On cooling to room temperature, a white precipitate of the desired product was deposited, which was collected by filtration and washed with diethyl ether (3.32 g, 62% yield). ^{1}H-NMR (300 MHZ, DMSO-d_6) δ (ppm): 11.70 (br s, 1H, NH); 11.11 (br s, 1H, NH); 7.94–7.90 (dd, 2H, J = 8 Hz, J = 1.6 Hz); 7.94 (dd, 2H, J = 1.76; 7.98 Hz); 7.46 (ddd, 2H, J = 1.71; 7.25; 8.35 Hz); 7.01–6.94 (m, 4H). ^{13}C-NMR (DMSO-d_6) δ (ppm): 165.80 (C–OH phenol); 158.56 (C═O amide); 134.08; 128.81; 119.23; 117.27 (C_{arom}); 114.96 (–C–CONH–). IR, ν (cm^{-1}): 3288, 3070, 2705, 1600, 1549, 1503, 1472, 1444, 1361, 1303, 1231, 1163, 1138, 1097, 1035, 955, 857, 780, 752, 688, 661. Anal. calc. (%) for $C_{14}H_{12}N_2O_4$: C 61.76; H 4.44; N 10.29. Found (%): C 61.30; H 4.58; N 10.41. Single crystals (colourless) suitable for X-ray structure determination (see ESI†) were obtained by slow diffusion of diethyl ether into a DMF solution of H_4**L**.

Synthesis of $(Fe^{III}Cl(DMF)_2)_2$L (1)

To a well-stirred solution of $FeCl_3{\cdot}9H_2O$ (595.7 mg, 3.64 mmol) in DMF (10 ml) was added 0.5 equiv. of H_4**L** (500 mg, 1.82 mmol). The red solution was left stirring for 5 hours in the dark at room temperature and 40 ml of diethyl ether was added to the solution. The dark red powder precipitated was filtered and washed with Et_2O. Red crystals of **1** that are suitable for X-ray diffraction were grown by diffusing diethyl ether into a DMF solution of **1** in the dark (0.94 g, 70% yield). Anal. calc. (%) for $C_{26}H_{36}Cl_2Fe_2N_6O_8$: C 42.02; H 4.88; N 11.31. Found (%): C 41.88; H 5.01; N 11.45.

Synthesis of $[Fe^{II}(DMF)_6][Fe^{II}Cl_4]$ (2)

To a well-stirred solution of $FeCl_3{\cdot}9H_2O$ (595.7 mg, 3.64 mmol) in DMF (10 ml) was added 0.5 equiv. of H_4**L** (500 mg, 1.82 mmol). The solution was left stirring for 5 hours at room temperature. The resulting red solution was degassed with nitrogen for 20 minutes to remove dissolved oxygen. Under an atmosphere of nitrogen, 5 ml of the solution was transferred to the lower part of a 20 ml closed glass test tube with a septum cap. The solution was exposed to natural light and when it had changed from red to colourless, the tube was filled with Et_2O. Colourless crystals (suitable for X-ray diffraction) of **2** and the free ligand H_4**L** were thus obtained and they have been separated with the help of a microscope for further

Table 1 Crystal data and refinement details for **1**, **2**, and H_4**L**

Compound	$Fe^{III}_2(L)Cl_2DMF_4$	$[Fe^{II}DMF_6][Fe^{II}Cl_4]$	H_4**L**
Formula	$C_{26}H_{36}Cl_2Fe_2N_6O_8$	$4[Fe_2C_{18}H_{42}N_6O_6Cl_4]$	$C_{14}H_{12}N_2O_4$
Colour	Red	Colourless	Colourless
Formula weight (g mol^{-1})	743.21	2768.3	272.26
Crystal system	Orthorhombic	Triclinic	Monoclinic
Space group	*Pbca*	$P\bar{1}$	$P2_1/n$
a [Å]	16.1661(10)	9.223(7)	8.3000(10)
b [Å]	9.4408(10)	18.6840(10)	6.2890(10)
c [Å]	21.396(4)	20.178(2)	12.1960(10)
α [°]	90.00	114.76(5)	90.00(5)
β [°]	90.00	92.29(5)	104.58(5)
γ [°]	90.00	91.81(5)	90.00(5)
V [Å^3]	3265.4(7)	3150(2)	616.11(19)
Z	4	1	2
Density (calc) [g cm^{-3}]	1.512	1.459	1.468
μ(Mo Kα) [mm^{-1}]	1.107	1.300	0.110
F(000)	1536	1440	284
Crystal size [mm]	0.14 × 0.09 × 0.09	0.12 × 0.10 × 0.08	0.15 × 0.08 × 0.08
Data collection			
θ Min–Max [°]	1.90–27.49	1.25–25.68	2.68–27.48
Data set [h, k, l]	−20/18, −7/12, −25/27	−11/10, −22/21, −23/24	−10/10, −8/7, −15/15
Total, Unique data	20 823, 3749	13 910, 10 078	2456, 1416
R(int)	0.0837	0.0258	0.0270
Observed data [$I > 2\sigma(I)$]	2386	6838	953
Refinement			
Reflections, parameters	3749, 200	10 078, 644	1416, 100
R_2, R_1	0.1031, 0.0552	0.0868, 0.0480	0.0738, 0.0429
wR_2, wR_1	0.1629, 0.1280	0.1230, 0.1053	0.1215, 0.1050
GooF	1.071	1.015	1.030
Maximum and average shift/error	0.000, 0.000	0.002, 0.000	0.000, 0.000
Min., max. residual density [e Å^{-3}]	−0.747, 0.994	−0.730, 0.770	−0.256, 0.206

studies. The crystalline blocks (stable in air for only a few minutes) of compound **2** have been selected by its slight tarnished coloration upon exposure to air compared to the free ligand. The quick surface coloration indicates the air sensitivity of the Fe^{II} species. The lack of chemical stability of complex **2** and its contamination with H_4**L** have hampered its chemical analyses.

Single crystal X-ray structure determination

Single crystals of the ligand H_4**L**, and the iron complexes **1** and **2** were mounted independently on glass fibers for intensity data collections on a Nonius Kappa-CCD area detector diffractometer (Mo Kα = 0.71073 Å). The details of data collection (DENZO)[32] and structure refinements are given in Table 1. The cell parameters were determined from reflections taken from one set of 10 frames (1.0° steps in phi angle), exposed for 20 seconds each. The structures were solved using direct methods and refined against F^2 using SHELXL97.[33,34] No absorption correction was applied. All non-hydrogen atoms were refined anisotropically and hydrogen atoms were introduced as fixed contributors (SHELXL97).

Crystallographic data (excluding structure factors) have been deposited at the Cambridge Crystallographic Data Centre under the deposition numbers CCDC 855119 (H_4**L**), 893268 & 893269 (iron complexes).

Electrochemistry

Electrochemical measurements were performed in *N*,*N*-dimethylformamide (DMF) (Sigma Aldrich; <0.1% H_2O) which was used as received. Electrochemical grade tetrabutylammonium hexafluorophosphate TBA(PF_6) (Fluka) was used as a supporting electrolyte. All electrochemical measurements were carried out at ambient temperature (20 ± 2 °C) in a conventional one compartment, three-electrodes cell. The working electrodes were platinum (2 mm diameter), glassy carbon (3.5 mm diameter) or a microelectrode of platinum (10 μm diameter). The counter electrode was a platinum wire and a second platinum wire was used as a pseudo-reference. The cell was connected to a PGSTAT 302 potentiostat (Eco Chemie, Holland). Prior to measurements, all the solutions were deoxygenated with argon. For complex **1**, the DMF solution was kept in the dark before measurements. When necessary ferrocene was used as an internal potential reference.

UV-visible spectroscopy

The UV-Visible spectra were recorded by transmission through *N*,*N*-dimethylformamide (DMF) (Sigma Aldrich; <0.1% H_2O) solutions of the compounds using a 8453 Agilent spectrophotometer and a standard 1 cm path length cell. The acid (commercial HCl) and base (distilled triethylamine) solutions were employed for the titration experiments.

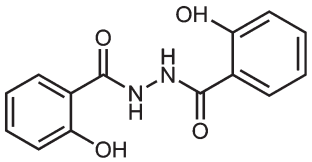

Scheme 1 Representation of *N*,*N*′-bis(salicyl)hydrazine (H_4**L**).

Results and discussion

H_4**L** is among a rare collection of ligands that can potentially carry charges from zero to four due to the easy deprotonation of both the phenol and the hydrazine moieties.[25] Furthermore, for both the neutral and the quadruply charged anion, one expects the geometry to be planar. Important with respect to the present work is this planarity and the divergent nature of the coordinating atoms to give two potentially symmetric meridional coordination sites. This aspect of the ligand has been demonstrated previously through its coordination with transition metals. Although the ligand is potentially able to coordinate metals into linear or even cyclic coordination networks, as known for a related ligand, none has been found so far. Our present study has confirmed the previously determined crystal structure of the ligand at a lower temperature.[25] This is consistent with the molecular structure determined by NMR spectroscopy in solution. Interestingly, these functional groups are involved in double intermolecular hydrogen bonding of ketone–alcohol pairs, O···H–O of 2.616 Å, between nearest neighbours leading to a two-dimensional supramolecular network. In addition, two equivalent intramolecular hydrogen bonds of amine–ketone pairs (N–H···O of 2.579 Å) exist. In this work, the synthesis and X-ray crystal structure of the first trivalent iron coordination complex – supported by *N*,*N*′-bis(salicyl) hydrazine ligand – is performed.

The reaction of one equivalent of the ligand H_4**L** with 2 equiv. of $FeCl_3$ in DMF results in a dense red solution where upon diffusion of ether it affords red crystals of **1** (Scheme 1) in good yield. An important procedure to be respected in this synthesis is the absence of natural light. This is because exposure of the red solution to natural light results in a fast discoloration to colourless (Fig. 1). The process can take as little as ten minutes for a solution of millimolar concentration. In the absence of light, dark red crystals suitable for single crystal X-ray analyses and other characterizations have been obtained by slow diffusion of diethyl ether into the DMF solution of **1** in air. The red crystals are stable in air and are soluble in H_2O, $CHCl_3$ and DMF but are insoluble in methanol, ethanol and diethyl ether.

The curiosity of the nature of the product(s) of this discoloration led us to the following. Crystallization tests were performed on the colourless solution obtained after exposure to natural light of **1** in DMF in sealed glass tubes. After a few hours of slow diffusion of diethyl ether into the irradiated DMF solution of **1**, colourless crystals start to form. Analyses of the X-ray data from different single crystals found the presence of two compounds, H_4**L** and **2**. With the help of a microscope, the two types of crystals were separated because the colourless crystalline blocks of **2** tarnished rapidly at the surfaces in air, indicating the sensitivity of the Fe^{II} species. In contrast, the crystals of H_4**L** do not change their colour.

Crystal structure of 1

1 crystallizes in the orthorhombic centro-symmetric space group *Pbca*. An ORTEP view of the molecular structure is depicted in Fig. 2. The asymmetric unit contains one half of the molecule of **1**, and the complete molecule $(FeCl(DMF)_2)_2L$ is generated by the inversion symmetry centred on the N–N bond. The unit cell has four molecules. **1** consists of a dinuclear Fe^{III} compound bridged symmetrically by one anionic ligand L^{4-}. The coordination of the ferric ion is pseudo-octahedral with two oxygen atoms (O1 and O2) and one nitrogen atom (N1) from the ligand in a meridional plane (Fig. 2), and the coordination sphere being completed by one chloride

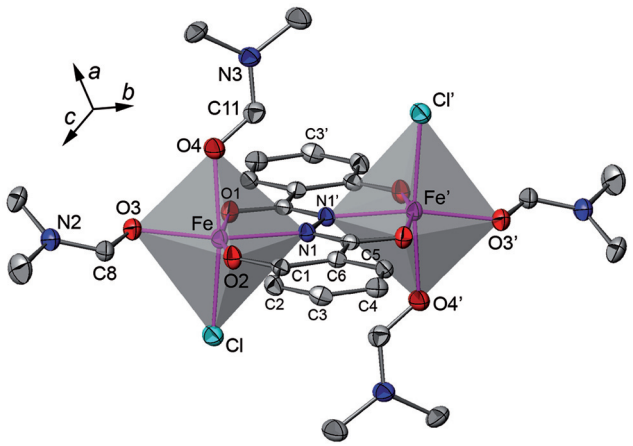

Fig. 2 ORTEP view of **1** with partial labelling. The polyhedra around Fe^{III} are represented in grey. The ellipsoids enclose 50% of the electronic density. Symmetry codes for equivalent positions are: $-x$, $-y+1$, $-z+1$.

Fig. 1 Discoloration of a DMF solution of **1** (10^{-3} M) under exposure to natural sunlight over a period of 10 minutes.

Table 2 Selected bond distances (Å) of known compounds and of the free ligand

Compound	H_4L	H_4L in $(Ni^{II}_2Lpy_6)\cdot H_4L$[26]	$Fe^{III}_2LCl_2(DMF)_4$	$(Co^{II}_2Lpy_6)(Co^{III}Cl_3py)_2$ [27]	$(Ni^{II}_2Lpy_6)\cdot H_4L$[26]	$(Ni^{II}_2Lpy_6)\cdot 2py$[26]	$(Zn_2Len_2)\cdot 2DMF\cdot 2H_2O$[28]
M–M			4.832	4.409	4.687	4.674	4.783
C=O (O1)	1.242	1.235	1.301	1.275	1.284	1.283	1.285
C–OH (O2)	1.362	1.356	1.339	1.325	1.339	1.302	1.325
N–N	1.379	1.378	1.401	1.368	1.409	1.408	1.396
M–O1			2.027	1.914	2.055	2.060	2.121
M–O2			1.898	1.852	2.049	1.989	2.049
M–N			2.037	1.849	1.974	1.955	2.003

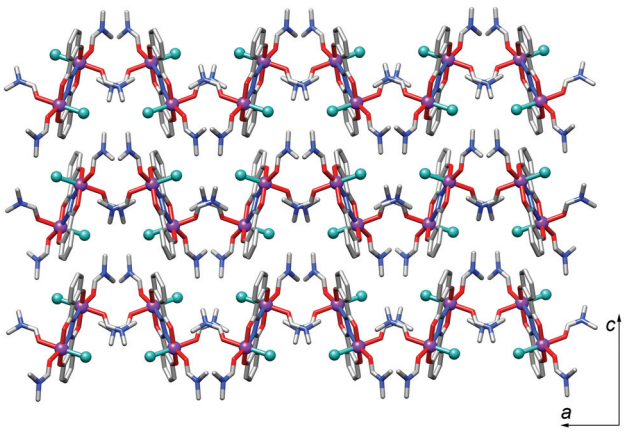

Fig. 3 Packing view of **1** (projection in the lattice plane *x*, 0, *z*). Iron atoms are represented as purple spheres and chloride atoms as blue green spheres.

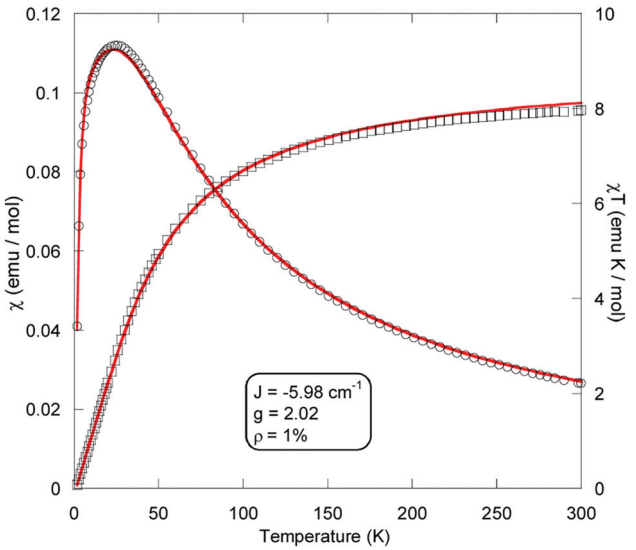

Fig. 4 Temperature dependence of χ (circles) and χT (squares) of **1**. The lines correspond to the best fit for a $S = 5/2$ dimer model.

atom and 2 DMF molecules (O3 and O4). The iron atoms are in *trans* position with respect to the N–N bond and are symmetry restricted to be in the plane of the ligand. The Fe–Fe′ distance is 4.832(1) Å. This core of the molecular structure of the present Fe^{III} compound is similar to those found previously containing Ni, Co and Zn ions.[26–28] For the latter the secondary ligands were neutral amine (pyridine or ethylenediamine) to balance the charge so that in all cases the molecules are neutral within the crystal structures. In the present case a chlorine atom bonded to each Fe^{III} satisfies the charge balance. By comparing the observed bond lengths of **1** to those of the free ligands (Table 2), we can note the following. First the ketone C=O distance is lengthened while the phenol C–O is shortened upon coordination, implying a transformation from a localised C=O and C–O picture in the pure ligand to a delocalisation of electron densities *via* a resonance effect upon deprotonation. While these distances are consistent for all the metal complexes reported, there are noticeable differences arising from the different valences and the ionic size of the cations as well as the nature of the other peripheral ligands. In all the compounds the geometry of the metals is pseudo-octahedral, and the M–O and M–N distances are normal except for those of cobalt, which are unexpectedly quite short. The M–O (ketone) is consistently longer than the M–O (alcohol). Surprisingly, the M–O (alcohol) bond lengths of the two compounds of nickel are very different, although they only crystallise with different solvates. No classical hydrogen bond has been detected. As non-classical hydrogen bonds, only one intermolecular C–H···π interaction has been pointed out (PLATON software[35]): C10–H10···(C1–C6)″ (″is related to the symmetry code $-x$, $\frac{1}{2} + y$, $\frac{1}{2} - z$); 2.866(1) Å between the hydrogen atom and the centre of the benzene ring (C1–C6) of an adjacent molecule, with an angle of 158(1)°. The corresponding packing diagram is represented in Fig. 3 and the main observation is the zigzag chains formed by the complexes along the ***a*** crystallographic axis, the (***a***,***c***) lattice plane. Although an infinite network is potentially expected, none have been characterized so far.

Magnetic properties of 1

With the two Fe^{3+} ($S = 5/2$) of the complex bridged by the short N–N entity and the lack of an extended network the present complex should potentially behave like a paramagnet with measurable intramolecular magnetic exchange. The magnetic measurements were undertaken on a sample of selected crystals of **1**, specifically to estimate the magnetic coupling between the two paramagnetic centres.

The magnetic moment represented as χT at room temperature of 7.95 emu K mol^{-1} (Fig. 4) is lower than that expected for two uncoupled Fe^{III} ions (8.75 emu K mol^{-1} assuming

g = 2.0). Upon cooling to 1.8 K, the χT product decreases gradually to near zero indicating the occurrence of intramolecular antiferromagnetic interaction. The temperature dependence of the magnetic susceptibility (χ) shows a gradual increase upon lowering the temperature to a maximum at 25 K. The data were fit using the following spin Hamiltonian where all parameters have their usual meaning and the spin operator $\hat{S}$ is defined as $\hat{S} = \hat{S}_{Fe1} + \hat{S}_{Fe2}$: $\hat{H} = -J\,\hat{S}_{Fe1}\cdot\hat{S}_{Fe2} + g\,\mathrm{H}\,\hat{S}$.[36]

Although reasonable fits were obtained, the low temperature data deviate from the theoretical curve. To improve the fits a certain amount ρ of paramagnetic impurity ($S_{impurity}$ = 5/2) has been considered. The best fit leads to the following values: $J = -5.98(3)$ cm^{-1}, $g = 2.02(1)$ and $\rho = 1\%$ with an agreement factor $R = 2 \times 10^{-4}$. The strength of the antiferromagnetic interaction ($J = -5.98(3)$ cm^{-1}) between the ferric ions in **1** is comparable to those available in the literature for complexes

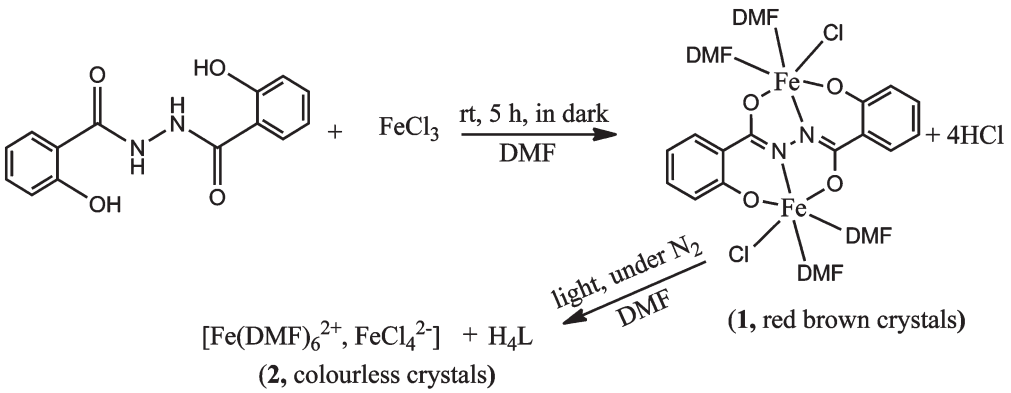

Scheme 2 Synthetic pathways for **1** and **2**.

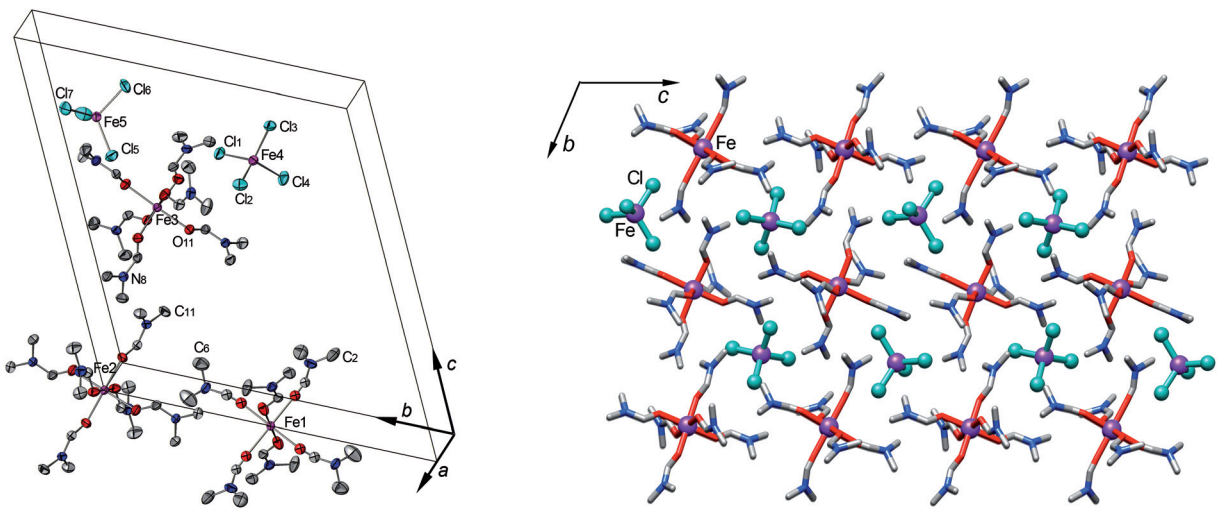

Fig. 5 Left – ORTEP view of the asymmetric unit of **2** with partial labelling scheme (the occupancy for Fe1 and Fe2 are 0.5). The ellipsoids enclose 50% of the electronic density. Right – packing view (projection in the lattice plane 0, y, z). Iron and chlorine atoms are represented as spheres.

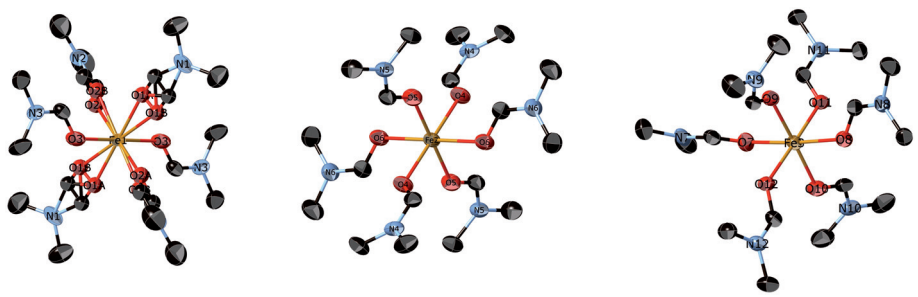

Fig. 6 Geometries of the three independent Fe cations in the crystal structure of **2**.

having a similar Fe^{III}–N–N–Fe^{III} exchange pathway, for example, ferric 24-Azametallacrown-8 complex[24a] (J = −3.93 cm^{-1}) and ferric 18-azametallacrown-6 compound[24b] (J = −3.38 cm^{-1}).

Crystal structure of 2

Single crystals of **2** have been picked quickly – under a microscope – from a collection of colourless single crystals, and mounted for intensity data collection. The crystalline blocks of **2** (stable in air for only few minutes) have been selected taking into account the surface coloration, indicating the air sensitivity of these Fe^{II} species (confirmed by the crystal structure obtained and described hereafter). The other crystalline blocks were also analyzed and the data analyses of the X-ray diffraction indicate that they correspond to that of H_4**L** (see also Scheme 2).

2 crystallises in the triclinic centro-symmetric space group $P\bar{1}$ (Fig. 5). The asymmetric unit contains five independent iron atoms, two of anion, $FeCl_4^{2-}$, and three of the cation, $Fe(DMF)_6^{2+}$ (Fig. 5 and 6). The anion has 100% occupancy and with their symmetry related counter parts there are four per unit cell. For the three cations (Fig. 6), two of them are in special crystallographic positions [Fe1: (0, $\frac{1}{2}$, 0), 25% occupancy; Fe2: (0, 0, 0), 12.5% occupancy] and one Fe3 (100% occupancy). While Fe1 and Fe2 have inversion centre and are ordered, Fe3 has no symmetry and the four equatorial DMF are disordered. Consequently, the cell contains one Fe1, one Fe2 and two Fe3 giving a total of four. Thus, the only possible charge balance is that the cation and the anion are double charged; that is all iron atoms are in the divalent state. This confirms the reduction of the Fe^{III} to Fe^{II} in solution. Furthermore, the decomplexation of the ligand has taken place in the process, which may be associated with weakening of the metal ligand coulombic forces in relation to those with DMF. It is important to note that the cationic complex has not been reported.[37] The DMF is coordinated through the oxygen atoms and the relative orientation of the $N(CH_3)_2$ units defines the overall geometry of the octahedra. However, there is no example of the cation in the literature for comparison but the Fe-O distances are all normal (2.090–2.162 Å) for the distorted octahedral geometry for each of the three cations observed. Concerning the anion, $FeCl_4^{2-}$, there are several examples in the literature and the geometries are invariably distorted tetrahedral, with all Fe–Cl distances and angles being normal (2.296–2.329 Å and 105.5–114.8° in the present case). No classical hydrogen bond has been detected in this crystal structure.

Electrochemical and spectroscopic characterizations

In order to collect data helping to understand the processes involved in the photoreduction of the Fe^{III} to Fe^{II} a series of additional experiments were undertaken. First we explored the properties of the ligand on its own by using photometric investigation.

Fig. 7 shows the concentration dependence of the spectrum of the ligand H_4**L** in DMF. Two overlapping absorption bands, centred at *ca.* 305 nm and 345 nm, were observed. The molar absorptivity of the 345 nm band increases with the concentration at the expense of the one at 305 nm. The observation of one isosbestic point is an indication of (at least) one equilibrium between two (or more) species. This can be due to agglomeration[38] of the molecules in solution at high concentration giving rise to the band at 345 nm that disappears upon

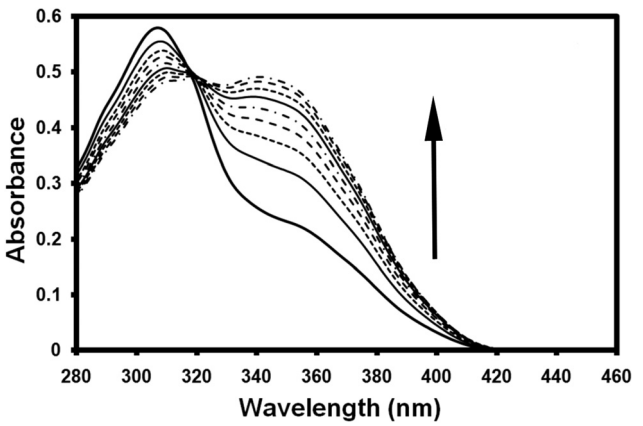

Fig. 8 Changes in the spectrum of H_4**L** (5×10^{-5} M) upon addition of triethylamine [0, 1, 2, 3, 4, 5, 6, 7 and 8×10^{-4} M].

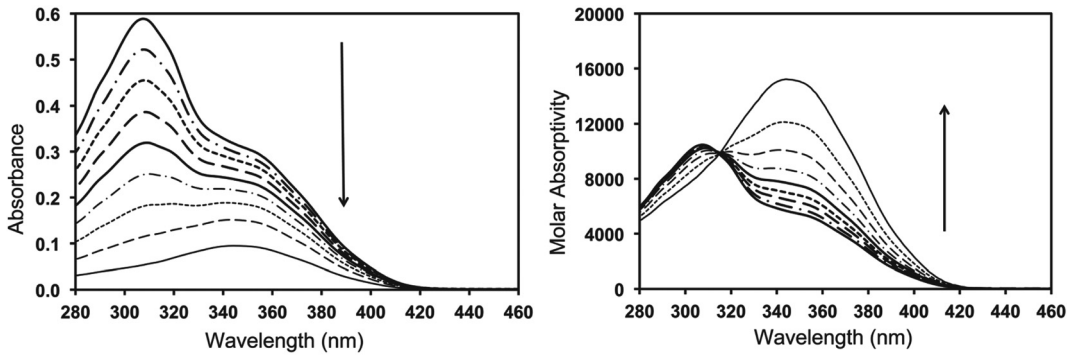

Fig. 7 Absorption spectra and its relative molar absorptivity of H_4**L** for different concentrations in DMF: 5.6, 5.0, 4.4, 3.7, 3.1, 2.5, 1.9, 1.3×10^{-5} M and 6.3×10^{-6} M (The arrow indicates the sense of the absorbance changes with decrease of the concentration).

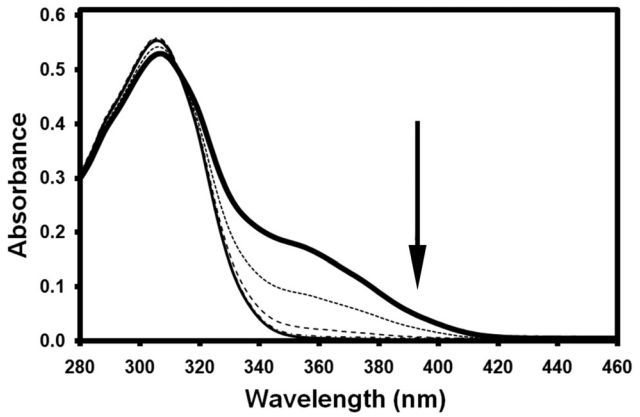

Fig. 9 Changes in absorption spectrum of H_4**L** (5×10^{-5} M) upon addition of HCl [0, 1.25, 2.5, 3.75 and 5×10^{-5} M].

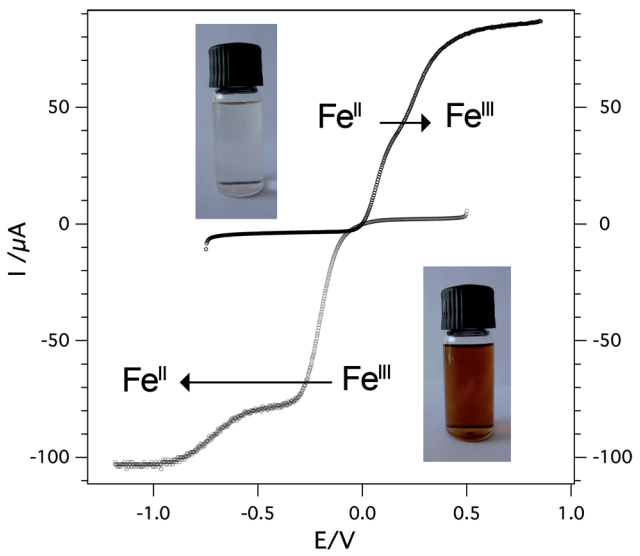

Fig. 10 Quasi-steady-state current-potential curves measured for the virgin Fe^{III} and the photoreduced Fe^{II} species at 1.25 mM in DMF (nBu_4NPF_6 0.15 M). Working electrode: glassy carbon. ν = 2 mV s^{-1} and rotation rate is 1000 rpm.

lowering the concentration. The second possibility is the formation of the deprotonated species in solution that is favoured by the presence of water acting as a base.

DOSY NMR (see Fig. S4 of ESI†) measurement provided an estimate of the hydrodynamic volume of the molecule in solution. The estimation of 285 Å^3 per molecule (based on Stock–Einstein relation) is close to 308 Å^3 obtained from crystallography and therefore we can exclude any aggregation under the conditions employed. It is important to note that the DOSY measurement was made with a concentration of H_4**L** of 1 mM, which is, at least, twenty times more concentrated than the solution used in the case of the spectroscopic studies. Supplementary measurements involving addition of a base (Fig. 8) and an acid (Fig. 9) to the solutions of the compounds were performed. Spectral changes associated with the addition of a base or an acid are in agreement with acid–base properties of the ligand (similar behaviour is observed for asymmetric ligands: see Fig. S1–S3 of ESI†).

The second experiment performed to elucidate the process of photoreduction was the electrochemistry of the Fe^{III}/H_4**L** solutions. First quasi-steady-state technique (Fig. 10) and secondly cyclic voltammetry were employed.

Fig. 10 shows the quasi-steady-state current-potential curves for the iron species in solution before and after light absorption. That of the starting red brown solution of Fe^{III} presents two reduction signals corresponding to probably the mononuclear species at −0.2 V and the dinuclear species at 0.7 V. After visible light irradiation no reduction wave was observed indicating the absence of ferric ions in this colourless solution. However, two near oxidation processes are observed (Fig. 6). These two waves can be attributed to the oxidation of the iron in the cation DMF–Fe^{II} and the anion Cl–Fe^{II} with possible Cl^-/DMF exchange during the Fe^{II} complexation/oxidation process, as demonstrated in the case of porphyrinic iron complexes.[39] The first wave most likely corresponds to Cl^-–Fe^{II} oxidation, being easier to oxidize, and the second wave (kinetic contribution) corresponds to the DMF–Fe^{II}

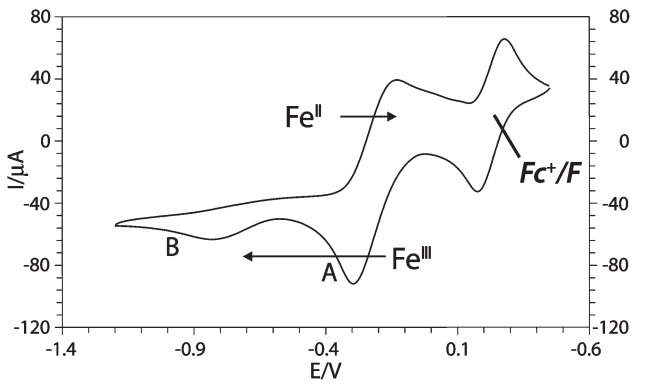

Fig. 11 Cyclic voltammogram of $2FeCl_3$ and H_4**L** 10 mM in DMF ($TBA(PF_6)$ = 0.15 M). Working electrode glassy carbon; v = 0.1 V s^{-1}.

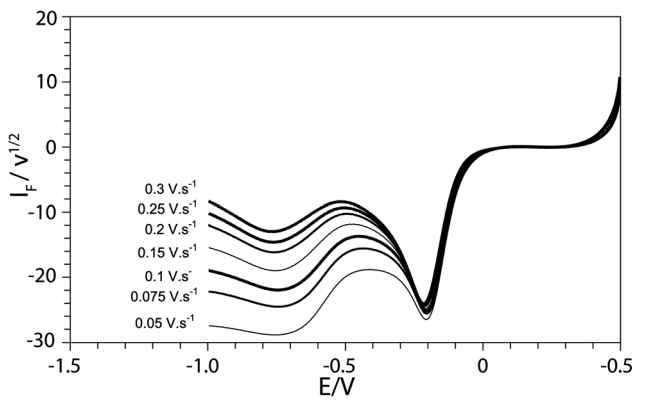

Fig. 12 Half cyclic voltammograms of $2FeCl_3$ and H_4**L** 1 mM at different scan rates in DMF ($TBA(PF_6)$ = 0.15 M). Working electrode: glassy carbon. I_F is the Faradic current obtained after subtracting the capacitive current.

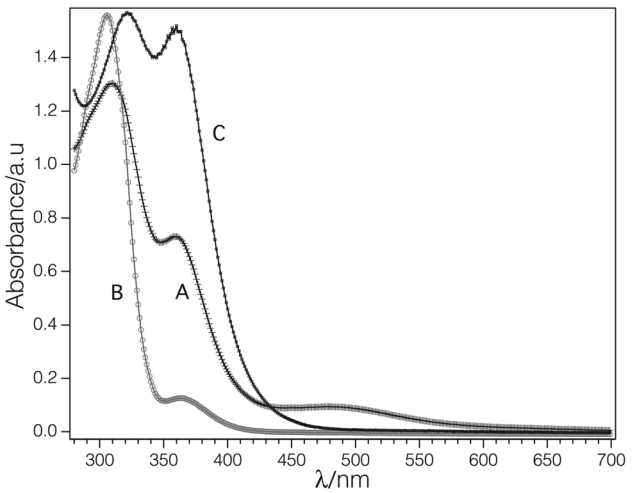

Fig. 13 Absorption spectra of (A) $Fe_2^{III}\mathbf{L}$, (B) $Fe^{II}/H_4\mathbf{L}$ obtained after light exposure of $Fe_2^{III}\mathbf{L}$, and (C) $FeCl_3$. All solutions are about 1 mM in DMF.

oxidation. These two oxidation processes possibly lead finally to the stable Cl^-–Fe^{III}/ligand compound giving rise, subsequently, to only one reduction step.

Concerning the reduction processes, one has to consider the Fe–L species present in the solution. In addition to the starting $FeCl_3$, both monomeric and dimeric complexes are also present. For the latter we can assume the complex found in the solid-state structure (see above), with one ligand coordinating two iron atoms, is present. The first reduction step is that of the monomers. The irreversible second reduction step (B in Fig. 11), which is not related to the ligand (see Fig. S7 of ESI†), may be assigned to the reduction of the second Fe^{III} of the dimers resulting in Fe^{II} complexes. As found by the crystallographic study of **2**, the cation $[Fe(DMF)_6]^{2+}$ and anion $[FeCl_4]^{2-}$ must be present. Thus, this observation suggests that at least for the second Fe^{III} complex, a chemical equilibrium exists between the ligand and solvated Fe^{III} and may be dependent on the first reduction step.

A further observation was the dependence of the intensity of the second reduction on the scan rate (Fig. 12). Without further speculation about the mechanistic reaction model, one can suppose that time (kinetic) is a pertinent parameter. While the current peak of reduction at A is independent of the scan rate, the current peak of reduction at B shows a noticeable dependence. This is an indication of a kinetic process associated with the first reduction step. It seems to confirm that the formation of dimers is a slow process; thus more of the mixed-valent compound is produced at a low scan rate.

The UV-visible absorption spectra of DMF solutions of $H_4\mathbf{L}$, $FeCl_3$ and their mixture have been recorded to shed some light on the photoreduction (Fig. 13). For $H_4\mathbf{L}$ and $FeCl_3$ the optical transitions are at energies higher than 450 nm. In contrast, that of a mixture of $H_4\mathbf{L}$ and $FeCl_3$ has an additional band centering at 500 nm, which gives the solution its characteristic red coloration. Given the matching of energy of the absorption band with that used for the photoreduction, it is highly conceivable that this band is the one absorbing the visible light and drives the reduction of the Fe^{III}, possibly *via* a transient mixed-valent state. Preliminary study indicates that the photoreduction also takes place in both THF and EtOH solvents.

After exposure of the ferric solution to natural light, the spectrum (B in Fig. 13) shows that the band at 500 nm disappears and the high-energy bands are at different energies to those of $FeCl_3$ but instead correspond to those of the ligand. This observation and the crystallographic study of **2** are consistent with the decomplexation of the dimeric Fe^{III} unit to Fe^{II} and the free $H_4\mathbf{L}$ ligand. A preliminary study of the EPR spectroscopy using a frozen DMF solution shows the formation of an organic radical (Fig. S13 of ESI†) upon irradiation with a laser delivering all the visible light (457–574 nm). The multiplicity of three, the *g*-values of 2.003, close to the free electron resonance, and the hyperfine constant A = 20 G are consistent with those of a free radical of DMF.[40] Thus a mechanism of photoreduction involving this radical is strongly possible.

To sum up the discussion of the pertinent results presented above and to explain the process of photoreduction in DMF solution, it is necessary to invoke also the crystallographic studies of the pure ligand and its salts with other transition metals. First it is important to comment on the formation of the crystals of the pure ligand after the irradiation of the Fe^{III}–$H_4\mathbf{L}$ solution. The observed results point out that the ligand is potentially acting as a catalyst promoting the formation of the dimer, which is subsequently photoreduced to produce the Fe^{II} in the solution while being liberated. Thus, it is conceivable that the reaction can be carried out to completion with much less than the equivalent quantities; an experiment which is in progress. Secondly, the results force us to conclude that the ability of the ligand to coordinate to transition metals of different ionic size and charge is quite subtle and variable. The works of Chen *et al.*[25–28] on Co, Ni and Zn suggest that the presence of pyridine and ethylenediamine stabilises the dimer formation by occupying the peripheral coordination. In their absence the dimeric Fe^{II} has not been observed. In our case, there is a subtle competition for coordination between the ligand and the other potential coordinating units in the solution; here, we note that in the absence of other ligands it is the DMF and the chloride ion that are coordinated to the Fe^{II}. In contrast for Fe^{III}, the ligand, chlorine and DMF are all favoured.

Conclusion

In this work, we have explored further the chemistry of the *N*,*N*′-bis(salicyl)hydrazide ligand ($H_4\mathbf{L}$) with $FeCl_3$ in DMF which has produced the dinuclear $(Fe^{III}Cl(DMF)_2)_2L$ complex. Its structure from single crystal X-ray diffraction provided an interesting comparison to the free ligand and other transition metal complexes, revealing the strength of the ligand towards different charged cations and their ionic radii in view of its quadruply charged state with bis-meridional coordination

sites. Fitting of the magnetic susceptibility data gave an antiferromagnetic coupling of $J = -6$ cm^{-1} for the rare Fe–N–N–Fe pathway. Interestingly, the $Fe^{III}Cl_3/H_4L$ solution in DMF is very sensitive to visible light and loses its red coloration in very short times in the absence of oxygen to form $[Fe^{II}(DMF)_6][Fe^{II}Cl_4]$. Crystallography of the products of this reaction and those known in the literature in conjunction with UV-vis spectroscopy and electrochemistry point to the fact that the photoreduction is promoted by the ligand and the active light receptor is the iron dimer in the solution. Furthermore, electrochemistry suggests that the process involves a mixed-valent Fe^{II}–Fe^{III} intermediate.

Acknowledgements

We thank the CNRS and the Ministère de la Recherche (France) for funding and for the financial support of the PhD of Nicolas Clément. We thank Région Alsace for the financial support of the PhD of Khaled Cheaib. We also thank Drs Jack Harrowfield (ISIS, Strasbourg) and Pierre Braunstein (UMR 7177, Strasbourg) for helpful discussions.

References

1 (*a*) D. Gatteschi, *Adv. Mater.*, 1994, **6**, 635; (*b*) A. Caneschi and D. Gatteschi, *Prog. Inorg. Chem.*, 1991, **39**, 331; (*c*) O. Kahn, *Molecular Magnetism*, VCH Publishers, New York, 1993; (*d*) *Metal–Organic and Organic Molecular Magnets*, ed. P. Day and A. E. Underhill, Spec. Publ. - R. Soc. Chem., Cambridge, UK, 2000, vol. 252; (*e*) *Molecular Magnetism, New Magnetic Materials*, ed. K. Itoh and M. Kinoshita, Gordon Breach-Kodansha, Tokyo, 2000; (*f*) *Magnetism: A Supramolecular Function*, ed. O. Kahn, Kluwer Academic Publishers, 1996.

2 M. Kurmoo, *Chem. Soc. Rev.*, 2009, **38**, 1353.

3 (*a*) R. M. Cornell and U. Schwertmann, *The Iron Oxides, Structure, Properties, Reactions, Occurrence and Uses*, VCH Publishers, Weinheim, Germany, 1996; (*b*) S. J. Blundell, *Magnetism in Condensed Matter*, Oxford University Press, 2001.

4 M. Kurmoo, H. Kumagai, S. M. Hughes and C. J. Kepert, *Inorg. Chem.*, 2003, **42**, 6709.

5 M. Verdaguer and G. Girolami, *Magnetism: Molecules to Materials V*, WILEY-VCH Verlag GmbH&KGaA, Weinheim, 2004.

6 J.-P. Zhang and X.-M. Chen, *Chem. Commun.*, 2006, 1689.

7 (*a*) M. Kurmoo and C. J. Kepert, *New J. Chem.*, 1998, **22**, 1515; (*b*) S. R. Batten and K. S. Murray, *Coord. Chem. Rev.*, 2003, **246**, 103.

8 (*a*) J. Ribas, A. Escuer, M. Monfort, R. Vicente, R. Cortes, L. Lezapma and T. Rojo, *Coord. Chem. Rev.*, 1999, **193–195**, 1027; (*b*) Y. F. Zeng, X. Hu, F.-C. Liu and X.-H. Bu, *Chem. Soc. Rev.*, 2009, **38**, 469.

9 (*a*) M. Kurmoo, *Mol. Cryst. Liq. Cryst.*, 2003, **379**, 271; (*b*) T. Lancaster, S. J. Blundell, F. L. Pratt and M. Kurmoo, *Phys. B*, 2003, **326**, 522.

10 (*a*) H. Tamaki, Z. J. Zhong, N. Matsumoto, S. Kida, M. Koikawa, N. Achiwa, Y. Hashimoto and H. Okawa, *J. Am. Chem. Soc.*, 1992, **114**, 6974; (*b*) S. Decurtins, *Philos. Trans. R. Soc. London, Ser. A*, 1999, **357**, 3025; (*c*) C. Mathoniere, C. J. Nuttall, S. G. Carling and P. Day, *Inorg. Chem.*, 1996, **35**, 1201.

11 (*a*) C. N. R. Rao, A. K. Cheetham and A. Thirumurugan, *J. Phys.: Condens. Matter*, 2008, **20**, 083202; (*b*) G. Ferey, *Chem. Soc. Rev.*, 2008, **37**, 191.

12 O. Kahn, *Adv. Inorg. Chem.*, 1995, **43**, 179.

13 M. Ruben, J. Rojo, F. J. Romero-Salguero, L. H. Uppadine and J.-M. Lehn, *Angew. Chem., Int. Ed.*, 2004, **43**, 3644.

14 S.-M. Peng, C.-C. Wang, Y.-L. Jang, Y.-H. Chen, F.-Y. Li, C.-Y. Mou and M.-K. Leung, *J. Magn. Magn. Mater.*, 2000, **209**, 80.

15 S. Vilminot, G. André, F. Bourée-Vigneron, P. J. Baker, S. J. Blundell and M. Kurmoo, *J. Am. Chem. Soc.*, 2008, **130**, 13490.

16 K. Mogilaiah, E. Anitha, K. S. Kumar and R. S. Prasad, *Ind. J. Chem. B*, 2011, **50B**, 126–128.

17 L. Saíz-Urra, M. P. González, Y. Fall and G. Gómez, *Eur. J. Med. Chem.*, 2007, **42**, 64–70.

18 K. Mogilaiah, M. Prashanthi and G. R. Reddy, *Synth. Commun.*, 2003, **33**, 3741–3745.

19 V. F. Shul'gin, E. A. Sarnit, O. V. Konnik, E. B. Rusanov, A. S. Bogomyakov, V. I. Ovcharenko and V. V. Minin, *Russ. J. Coord. Chem.*, 2012, **38**, 44–49.

20 G. I. Mustata, A. Brigo and J. M. Briggs, *Bioorg. Med. Chem. Lett.*, 2004, **14**, 1447, 22, 1447–1454.

21 C. Beghidja, G. Rogez, J. Kortus, M. Wesolek and R. Welter, *J. Am. Chem. Soc.*, 2006, **128**, 3140.

22 (*a*) N. Bouslimani, N. Clément, G. Rogez, P. Turek, M. Bernard, S. Dagorne, D. Martel, H. N. Cong and R. Welter, *Inorg. Chem.*, 2008, **47**, 7623; (*b*) N. Clément, C. Toussaint, G. Rogez, C. Loose, J. Kortus, L. Brelot, S. Choua, S. Dagorne, P. Turek and R. Welter, *Dalton Trans.*, 2010, **39**, 4579.

23 R. Welter, *Pat.*, WO 2009/130562 A1, 2009; "Method and device for producing and storing energy".

24 (*a*) S. Lin, S.-X. Liu, Z. Chen, B.-Z. Lin and S. Gao, *Inorg. Chem.*, 2004, **43**, 2222; (*b*) S. Lin, S.-X. Liu and B.-Z. Lin, *Inorg. Chim. Acta*, 2002, **328**, 69.

25 Y. T. Chen, D. C. Li, D. Q. Wang and Y. H. Zhu, *Acta Crystallogr., Sect. E: Struct. Rep. Online*, 2007, **64**, o120.

26 Z. Y. Wang and S. X. Liu, *Acta Crystallogr., Sect. E: Struct. Rep. Online*, 2007, **63**, m2503.

27 Y. T. Chen, J. M. Dou, D. C. Li, D. Q. Wang and Y. H. Zhu, *Acta Crystallogr., Sect. E: Struct. Rep. Online*, 2007, **63**, m3129.

28 Z. Y. Wang and S.-X. Lin, *Acta Crystallogr., Sect. E: Struct. Rep. Online*, 2007, **63**, m3105.

29 V. Bazani and V. Carassiti, *Photochemistry of Coordination Compounds*, Academic Press, London and New-York, 1970.

30 J. Sima and J. Makanova, *Coord. Chem. Rev.*, 1997, **160**, 161.
31 Ligand synthesis: (*a*) H. Zhao and T. R. Burke Jr, *Tetrahedron*, 1997, **53**, 4219; (*b*) P. V. Bernhardt, P. Chin, P. C. Sharpe, J. C. Wang and D. R. Richardson, *JBIC, J. Biol. Inorg. Chem.*, 2005, **10**, 761.
32 *Kappa CCD Operation Manual*, Nonius B. V., Delft, The Netherlands, 1997.
33 G. M. Sheldrick, *SHELXL97, Program for the Refinement of Crystal Structures*, University of Gottingen, Germany, 1997.
34 R. Welter, The Crystalbuilder Project, *Acta Crystallogr., Sect. A: Found. Crystallogr.*, 2006, **62**, s252.
35 A. L. Spek, PLATON software, *J. Appl. Crystallogr.*, 2003, **36**, 7.
36 C. J. O'Connor, *Magnetic Susceptibility Measurements. Progress in Inorganic Chemistry*, 29, ed. S. J. Lippard, 1982, p. 203.
37 A. L. Rheingold and B. S. Hammes, *Private Communication*, 2002, (CCDC 187571), Contribution from Department of Chemistry and Biochemistry, University of Delaware, DE 19716, USA.
38 L. Antonov, G. Gergov, V. Petrov, M. Kubista and J. Nygren, *Talanta*, 1999, **49**, 99–106.
39 D. Lexa, M. Momenteau, P. Rentien, G. Rytz, J. M. Savéant and F. Xu, *J. Am. Chem. Soc.*, 1984, **106**, 4755.
40 I. A. Shkrob and T. W. Marin, *J. Phys. Chem. A*, 2012, **116**, 1746–1757.